Applied Thermal Engineering 175 (2020) 115316

Contents lists available at ScienceDirect

Applied Thermal Engineering

journal homepage: www.elsevier.com/locate/apthermeng

Exergetic investigation and optimization of arc shaped rib roughened solar air heater integrated with fins and baffles

P.T. Saravanakumar[a], D. Somasundaram[b,*], M.M. Matheswaran[c]

[a] Department of Automobile Engineering, Hindusthan Institute of Technology, Coimbatore, Tamil Nadu 641032, India
[b] Department of Mechanical Engineering, Sri Ramakrishna Institute of Technology, Coimbatore, Tamil Nadu 641010, India
[c] Department of Mechanical Engineering, Jansons Institute of Technology, Coimbatore, Tamil Nadu 641659, India

HIGHLIGHTS

- Analytical study of roughened SAH with fins and baffles is investigated.
- Exergy efficiency is evaluated based on exergy destruction and losses.
- Genetic algorithm optimises parameters with maximum exergy efficiency of 5.2%.
- Optimised mass flow rate is 0.012 kg/s and performs better up to 0.042 kg/s.

ARTICLE INFO

Keywords:
Solar air heater
Exergetic efficiency
Genetic algorithm
Arc shaped roughness
Extended surface

ABSTRACT

Present work focuses on exergetic performance and parameter optimization of arc shaped rib roughened solar air heater integrated with fins and baffles. Theoretical analysis based on exergy loss has been considered to study the effect geometrical and operating parameters on exergy efficiency of SAH. Energy and exergy balance equations have been solved by developed code using MATLAB. Variations of exergy destruction and losses with reference to decisive parameters are presented. Further, Genetic algorithm has been invoked to optimize the design and operating parameters of SAH. It is revealed that the maximum exergy efficiency of proposed SAH is 5.2% at optimized conditions. From the plots, it is evident that the maximum exergy is obtained for number of fins of 8, baffle length of 0.2 m, baffle width of 0.015 m and mass flow rate of 0.012 kg/s. Simulations results of present model for proposed SAH has been validated with models available in the literature and found to be in good agreement.

1. Introduction

The rate of energy consumption increases due to industrial development and population growth. It makes economic pressure and environmental damages in the form of global warming, acid rain, Ozone layer depletion etc. Global energy potential demand is about 11,941 EJ/year at the end of 2050 as reported by Renewable Energy Policy Network for the 21st Century (REN21). An energy scenario focuses on technology transfer towards 100% renewable in the near future. Considering various renewable sources, solar thermal energy contribution in meeting global energy demand is about 388 TWh of heat [1].

As industries demands more heat for processing various products, solar air heaters are mostly developed with various configurations. Performance of Solar air heater (SAH) has been improved by detailed experimental and theoretical studies conducted by many researches in the literature. SAH has low heat transfer coefficient due to thermo physical properties of air and formulation of viscous sub layer. In order to improve the thermal performance, novel techniques suggested as in the literature, will be discussed.

Kumar et al. [2] conducted experiment to improve the thermo hydraulic performance of SAH with discrete multi V rib. It is found that the heat transfer rate has been enhanced in the range of 5.58 to 6.2 times compared with conventional SAH. Compound turbulators are used to increase the heat transfer rate with pressure drop as a penalty. Aharwal et al. [3] developed empirical correlation for heat transfer coefficient and friction factor as a function of wedge angle and relative groove position. Skullong et al. [4–6] carried out experimentation for thermal performance improvements of SAH with different configuration of artificial roughness. It is found that the thin rib turbulators

* Corresponding author.
E-mail addresses: ptscfd@gmail.com (P.T. Saravanakumar), soms.iitm@gmail.com (D. Somasundaram), madhume01@gmail.com (M.M. Matheswaran).

https://doi.org/10.1016/j.applthermaleng.2020.115316
Received 4 November 2019; Received in revised form 30 March 2020; Accepted 8 April 2020
Available online 22 April 2020
1359-4311/

Nomenclature

A_{pl}	Surface area of collector (m^2)
A_{baf}	Baffle area (m^2)
$A_{b\text{-}fin}$	Extended surface area (fins) (m^2)
C_{pa}	Specific heat of air (J/kg K)
D_h	Rectangular duct hydraulic diameter (m)
$\dot{E}$	Exergy (W)
e/Dh	Ratio between Rib height-to-duct hydraulic diameter
fr	Friction factor of air flow path
g	Acceleration due to gravity (m^2/s)
h_{cn}	heat transfer co efficient due to Convection (W/m^2 K)
h_{rn}	heat transfer co efficient due to Radiation (W/m^2 K)
h_{wd}	heat transfer coefficient between wind and glass surface (W/m^2 K)
h_{fin}	Height of the extended surface
k_a	Thermal conductivity of air (W/m K)
k_{fin}	Thermal conductivity of the extended surface
L_d	Length of the collector (m)
L_B	Baffle plate length
$\dot{m}_a$	Rate of air flow (kg/s)
Nu	Nusselt number
N_o	Number of fins
P_{mech}	Mechanical power consumption (W)
Q_{us}	Beneficial heat gain (W)
$\dot{Q}_r$	Radiative heat transfer
$\dot{Q}_c$	Convective heat transfer
Re	Reynolds Number
S	Solar radiation (W/m^2)
SAH	Solar Air Heater
GA	Genetic algorithm

Subscripts

amb	Ambient air
be	Back plate
gc	Glass cover
fi	air inlet to the channel
ins	Insulation
f	Air in the channel
fo	air out to the channel
pl	Absorber plate
sy	Sky
in	inlet
out	Outlet
Opt-loss	Optical loss
Q-loss	Heat loss to the surrounding
fr-loss	Fluid frictional losses
T_{Pl}-T_{sun} loss	Destruction loss between plate and sun
T_{Pl}-T_{fl} loss	Destruction loss between plate and air flow through duct
T	Temperature (K)
t_{fin}	Thickness of the extended surface
U_{be}	heat transfer coefficient for Bottom loss (W/m^2 K)
UL	Total heat loss coefficient (W/m^2 K)
V_{wd}	Wind Velocity (m/s)
W_d	Width of the air flow path
w_B	Baffle plate width
Z_2	Height of air heater channel (m)

Greek symbols

α	Absorptivity
ΔP_a	Drop in pressure through air flow duct (N/m^2)
η_I	Thermal Efficiency of SAH (%)
η_{eff}	Effective (or) Thermo hydraulic Efficiency of SAH
η_{fin}	Efficiency of the Extended surface
η_{ex}	Exergy efficiency of SAH
η_{baff}	Efficiency of the Baffle
ε	Emissivity
μ_a	Viscosity of air (kg/m s)
φ	Angle of tilt for air heater (°)
Ψ_x	dimension less parameter
ρ_a	Density of air (kg/m^3)
σ	Stefan's Boltzmann constant (W/m^2 K^4)
τ	Transmissivity of glass cover

increases thermal enhancement factor (TEF) around 3–7%. Further they used combined wavy-groove and delta-wing vortex generator to improve the convective heat transfer rate and found that the TEF is around 2.24. Further, wavy grooves incorporated with pairs of trapezoidal-winglets were used to enhance TEF by 43% above grooved only SAH. The correlation was developed to predict the nusselt number and friction facto as function of operating and geometry conditions for the all the configurations.

The SAH equipped with ribs is investigated experimentally to find out the heat transfer and pressure drop by Salameh et al. [7]. It shows that the pressure drop is the same for all the shape of the ribs while dimpled rip provides better heat transfer rate and grooved rip records high performance index. The multi V -down perforated baffles are tested experimentally with SAH in order to investigate heat transfer performance. It shows that the thermal efficiency is maximum at the relative baffle width of 5 and thermo hydraulic performance is better than that of other shaped baffles [8]. Ravi et al. developed correlation for nusselt number and friction factor for double pass SAH with discrete multi V shaped and staggers rib roughness. In this work, thermal performance is increased by 4.52 times and friction factor of about 3.13 time s compared with convention double pass SAH [9].

For optimizing the SAH design and operating conditions, quality based analysis is more reliable. Sahu et al. [10] used analytical investigation to optimize the geometrical parameters for SAH with arc shaped roughness. From the exergy efficiency curves, it is found that enhancement in exergy efficiency of 56% compared with smooth plate SAH. Kumar et al. [11] used twisted rib roughness to optimize the energy and exergy efficiency. It is reported that the improvement in thermal efficiency of 1.81, effective efficiency of 1.79 and exergetic efficiency of 1.81 times respectively. In this study [12], thermal and economies and environmental influence on the performance improvement of SAH is carried out experimentally by Abuska et al. It is found that the SAH with copper v-groove shows the better heat transfer rate with lower pressure drop. Simple payback period and enviro-economic are found to be average of 4.5 years and 5$/year. Further , SAH efficiency is enhanced by conical shaped roughness and it is found that the maximum exergy efficiency is 19.3% at lower mass flow rate of 0.04 kg/s [13]. Matheswaran et al. [14,15] numerically calculated the exergetic and enviro-economic performance of double duct SAH with arc shaped roughness and revealed that the reduction in CO_2 emission of 2.1 times compared with conventional SAH. Further, roughness parameters multiple arc shape protrusion based on exergetic performance of SAH.

It is reviewed that the use of artificial roughness improves the heat transfer by enhancing the heat transfer coefficient. It is also known that heat transfer can also be increased by increasing surface area are by providing fins and baffles. Fins and absorber plate attached with steel wire is used for enhancing the performance of SAH. In this study, the effect of the mass flow rate of air is studied experimentally [16] and found that the increase in air mass flow rate enhances the efficiency for

double pass solar air heater. Reynolds-averaged Navier–Stokes equations are used to analyze the solar air heater and find out the optimum shape of the obstacles that are to be attached with SAH [17]. Four different obstacles are used and tested and it is found that the pentagon obstacle has better heat transfer characteristics. Experimental investigation on energy and exergy analysis of flat plate SAH with various obstacles has been carried out by Akpinar et al. [18]. It is found that the solar radiation, surface geometry and air flow line influence the performance of SAH. Lowest efficiency due to irreversibility is estimated for SAH without obstacles.

Broken multi type v- baffles are used to increase the thermal hydraulic performance in SAH. Experiments show the significant impact of baffle on thermal performance for different geometrical and flow parameters [19]. Steady state mathematical model reveals the effect of number of fins and baffles on effective efficiency of SAH and concludes that the baffle width has significant impact on performance when the flow is fully turbulent [20]. Absorber plate with fins and baffles are used to enhance the thermal performance of single pass solar air heater. Geometry parameters are varied to find the energy and effective efficiencies with external recycle device. It is found out that attaching both fins and baffles with recycle boost the energy efficiency but larger baffle with and lower distance between baffles increases the pressure drop. It is recommended to use only fins at high mass flow rate and recycle ratio to enhance performance of SAH [21]. Saravanakmar et al. [22] developed MATLAB code for investigating the thermo hydraulic performance of SAH with fins and baffles integrated with arc shaped roughness. It is concluded that the energy and effective efficiency are enhanced by 28.3% and 27.1% compared with SAH with arc shaped roughness.

Exergy and energy performance of SAH with fins is compared with SAH without fins for various air flow conditions. It is concluded that SAH with fins and heater with double glass cover provides effective heat transfer and lower mass flow rate of air is preferred when temperature difference between outlet and inlet air is important [23]. In addition to fins, baffles are also used to increase the thermal performance of SAH. Recently porous baffles are effectively sued to increase the heat transfer rate between the plate and air. Metal foam and perforated baffles are widely used to increase convective heat transfer between flowing fluid and heated surfaces [24]. Bayrak et al. [25] concluded from the experiment that the staggered porous baffles yields the maximum exergy efficiency of 54.54% due to lower irreversibility. Sabzpooshani et al. [26] analytically investigated exergetic performance of SAH with fins and baffles. In this study, it is revealed that lower mass flow rate, attaching the baffles enhances the exergy efficiency as trend is reversed at higher baffle width. Energy and exergy performance of SAH depends on various parameters. In order to optimize the design and performance parameters, Genetic algorithm (GA) [27], artificial Bee colony (ABC) [28], artificial neural network (ANN) and response surface methodology (RSM) [29,30] have been applied.

From the above literature review, it is ensured that the exergetic performance of solar air heater is enhanced by artificial roughness, fins and integration of fins and baffles. It is found that the combining above mentioned techniques is novel method of improving the exergetic performance of SAH. In this research work, arc shaped rib roughened SAH integrated with fins and baffles are exergetically investigated. Based on exergy loss, genetic algorithm is invoked for optimizing the design parameters of SAH such as width of the baffle (W), length of the baffle and number of fins (N) and operating parameters such as mass flow rate. Validation of proposed study has been carried out with literature results and a reliable agreement has been observed.

2. Description of theoretical model

Fig. 1a shows the core components of solar air heater. In this SAH, solar radiation falling on the glass cover is transmitted to the absorber plate. Heat loss from the top surface of the absorber plate is minimized by the same glass cover. Beneath the absorber plate, the artificial roughness made up of arc shaped wire is attached to disintegrate formulation of laminar sub layer. In addition, the fins are attached with absorber plate as well as back pate along the flow direction thereby more heat is transferred to air. Attached fins provide channeled flow of air as it is equally placed along the width of SAH. Further, the heat transfer enhancement could be achieved by attaching baffles with fins across air flow direction. Back plate provides the flow path and supports the fins attached with baffles. Heat loss to atmosphere is prevented by providing the insulation made up of glass wool as shown in Fig. 1b.

Fig. 1c shows the detailed depiction of fluid flow phenomenon over the absorber plate. When the air enters the SAH, the flow is channeled by the arrangement of fins equally spaced along the width. Flowing fluid is disturbed by staggered baffles where by the more turbulence is induced by local swirl. In addition to this, the artificial roughness will also induce chaotic flow by means of flow separation.

Assumptions

The following assumptions are invoked to carry out the analytical model [15,33].

1. SAH operates at steady state condition.
2. Flow through the SAH is one dimensional.
3. SAH is perfectly sealed in order to avoid air leaks.
4. Thermo physical properties of components of SAH are assumed to be constant.
5. Sky can be considered as black body.
6. Contact resistance due to attachments of fins and baffles is neglected.

2.1. Development of energy balance equations for SAH

The energy transfer happened on the glass cover is described by the Eq. (1) and reformulated form is shown in Eq. (2). From the equations, the glass cover gains heat energy which was liberated from the sun and absorber plate by integrating the convection and radiation mode of heat transfer. Then the part of absorbed energy by the glass cover is transferred to the sky and remaining heat is taken by the flowing wind as top heat loss. The final energy balance equation for glass cover is written as

$$\dot{Q}_{r,sun-gc} + \dot{Q}_{c,\,\mathrm{pl-}\,gc} + \dot{Q}_{r,\,pl\,-\,gc} = \dot{Q}_{\mathrm{c,\,gc-amb}} + \dot{Q}_{r,\,\mathrm{gc-sy}} \tag{1}$$

$$(h_{wd} + h_{r,\,gc\,-\,sy} + h_{r,\,pl\,-\,gc} + h_{cn,\,\mathrm{pl-}\,gc})T_{gc} - (h_{cn,\,\mathrm{pl-}\,gc} + h_{rn,\,pl\,-\,gc})T_{pl} = (\alpha_{\mathrm{gc}}S + h_{wd}T_{am} + h_{rn,\,gc\,-\,sy}\mathrm{T_{sy}}) \tag{2}$$

The energy balance equation for the absorber plate is described by the Eq. (3) and its deduced form is shown in Eq. (4). The absorber plate is heated by the solar irradiation falling on it. Then this energy is distributed to flowing air and other solar air heater components by the convection and radiation mode of heat transfer. The energy transfer to air is taken as useful heat gain and the later is energy loss parameter from the SAH. The final energy balance equation for absorber plate is rewritten as

$$\dot{Q}_{r,sun-pl} = \dot{Q}_{cn,pl\,-\,\mathrm{gc}} + \dot{Q}_{rn,pl\,-\,\mathrm{gc}} + \dot{Q}_{cn,pl\,-\,\mathrm{f}} + \dot{Q}_{rn,pl\,-\,\mathrm{be}} \tag{3}$$

$$\alpha_{\mathrm{pl}}\tau_{\mathrm{gc}}S = -(h_{cn,pl\,-\,\mathrm{gc}} + h_{rn,pl\,-\,\mathrm{gc}})\mathrm{T_{gc}} + (h_{cn,pl\,-\,\mathrm{gc}} + h_{rn,pl\,-\,\mathrm{gc}} + h_{c,pl\,-\,\mathrm{f}} + h_{r,pl\,-\,\mathrm{be}})\mathrm{T_{pl}} - \psi_x h_{cn,pl\,-\,\mathrm{f}}\mathrm{T_f} - h_{rn,pl\,-\,\mathrm{be}}\mathrm{T_{be}} \tag{4}$$

The air flows through the SAH duct and absorbs the heat energy from the absorber plate and back plate. The energy balance equation for the process is described in Eq. (5) and its reformulated form is shown in Eq. (6)

$$\dot{Q}_{u,f} = \psi_x \dot{Q}_{c,pl\,-\,\mathrm{f}} + \dot{Q}_{c,\,\mathrm{be-f}} \tag{5}$$

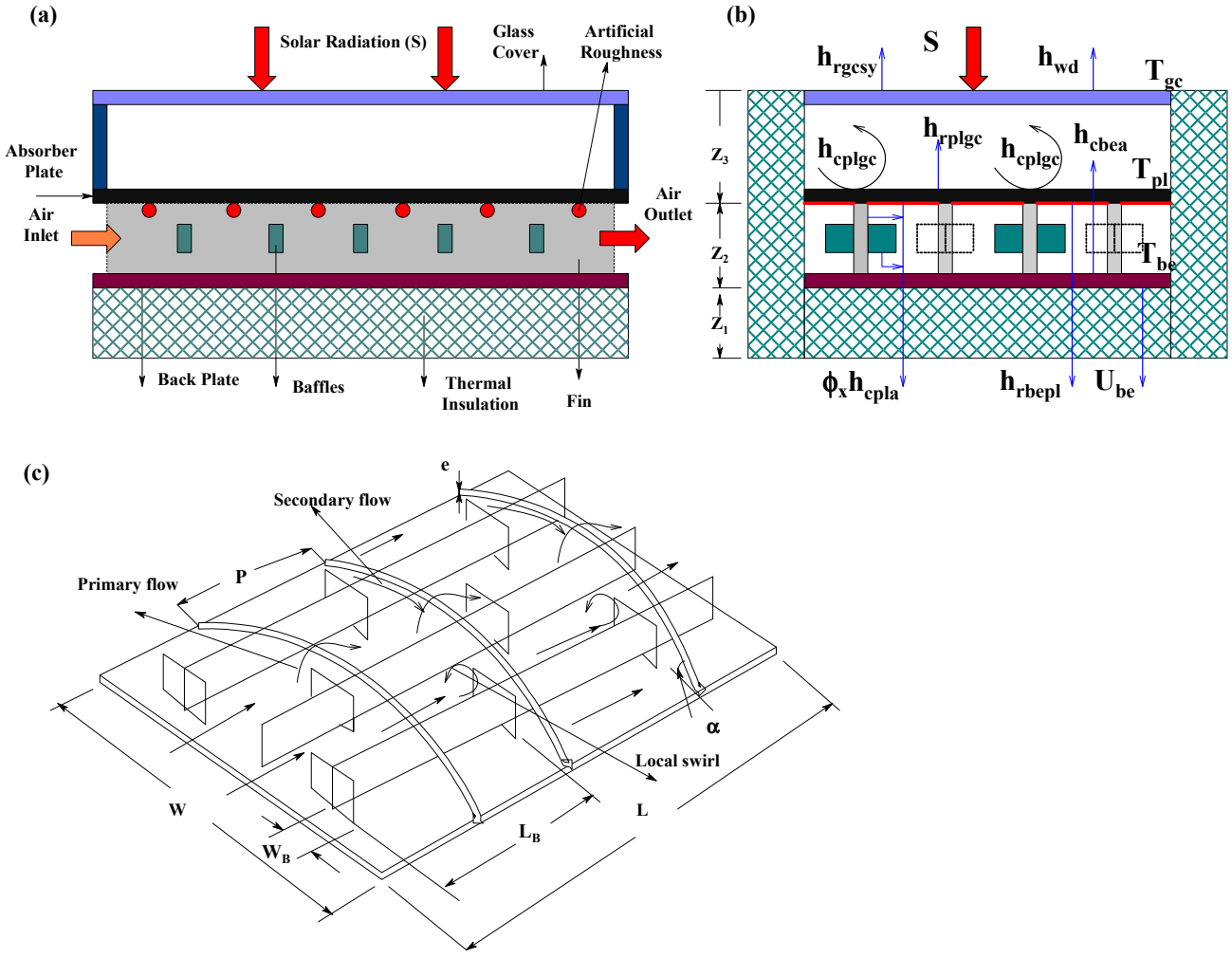

Fig. 1. Schematic diagram of SAH (a) Cross section view (b) Energy Balance (c) Flow over absorber plate.

$$\left(\frac{-2\dot{m}CT_{fi}}{A_{pl}}\right) = \psi_x h_{c,pl\text{-}f}\,T_{pl} - \left(\psi_x h_{cn,pl\text{-}f} + h_{cn,be\text{-}f} + \frac{2\dot{m}C}{A_{pl}}\right)T_f + h_{c,be\text{-}f}\,T_{be} \tag{6}$$

$$\psi_x = 1 + \frac{A_{fin}}{A_{pl} - A_{b-fin}}\eta_{fin} + \frac{A_{baf}}{A_{pl} - A_{b-fin}}\eta_{baf} \tag{7}$$

$$\eta_{fin} = \frac{\tanh(mh_{fin})}{mh_{fin}} \tag{8}$$

In this work, the presence of fins and baffles enhances the flow turbulences and convective heat transfer coefficient. The dimension less parameter Ψx is introduced to incorporate this effect on the energy balance equation. The required parameters are evaluated to calculate the values of Ψx, using the equations from (7) to (10) [22].

$$m = \sqrt{\frac{2(h_{cn\ pl\text{-}a}(L_d + t_{fin})}{k_{fin}L_d t_{fin}}} \tag{9}$$

$$\eta_{baf} = 15.583\left[\frac{W_B}{D_h}\right]^{0.0518}\left[\frac{L_d}{L_B}\right]^{-0.2247} \tag{10}$$

The energy transfer on back plate is described by the Eq. (11) and its reformulated form is shown in Eq. (12). It is clear that the back plate supplies part of energy, received from the absorber plate, to the working fluid and the remaining heat is lost to the ambient as bottom loss as shown in Fig. 1.

$$\dot{Q}_{r,pl-be} = \dot{Q}_{c,be\text{-}f} + \dot{Q}_{be\text{-}am} \tag{11}$$

$$h_{rn,pl-be}T_{pl} + h_{cn,be\text{-}f}T_f - (h_{rn,pl-be} + h_{cn,be\text{-}f} + U_{be})T_{be} = -U_{be}T_{amb} \tag{12}$$

2.2. Temperature calculations of SAH components

To calculate the temperature of the SAH components, Eqs. (2), (4), (6) and (10) are rewritten as follows

$$T_{gc} = \frac{\alpha_{gc}S + h_{wd}T_{amb} + h_{rn,gc\text{-}sy}T_{sy} + (h_{cn,pl\text{-}gc} + h_{rn,pl\text{-}gc})T_{pl}}{(h_{wd} + h_{rn,gc\text{-}sy} + h_{rn,pl\text{-}gc} + h_{nc})} \tag{13}$$

$$T_{pl} = \frac{\alpha_{pl}\tau_{gc}S + (h_{cn,pl\text{-}gc} + h_{rn,pl\text{-}gc})T_{gc} + \psi_x h_{cn,pl\text{-}f}T_f + h_{rn,pl\text{-}be}T_{be}}{(h_{cn,pl\text{-}gc} + h_{rn,pl\text{-}gc} + h_{cn,pl\text{-}f} + h_{rn,pl\text{-}be})} \tag{14}$$

$$T_f = \frac{\left(\frac{2\dot{m}C_{pa}T_{fi}}{WL}\right) + \psi_x h_{cn,pl\text{-}f}T_{pl} + h_{cn,be\text{-}f}T_{be}}{\psi_x h_{cn,pl\text{-}f} + h_{cn,be\text{-}f} + \frac{2\dot{m}C_{pa}}{WL}} \tag{15}$$

$$T_{be} = \frac{U_{be}T_{amb} + h_{rn,pl-be}T_{pl} + h_{cn,be\text{-}f}T_f}{(h_{rn,pl-be} + h_{cn,be\text{-}f} + U_{be})} \tag{16}$$

Further, the equations require thermo physical properties and heat transfer coefficients. The correlations for finding these values are described in the subsequent sections.

2.3. Thermo physical properties and heat transfer co efficient for simulation

The air temperature causes variations in thermo physical properties. To evaluate these values the following correlations are used as a function of mean air temperature [15,33].

$$C_p = 1.0057 + 0.000066(T_{avg} - 27) \tag{17}$$

$$\rho_a = 1.1774 - 0.00359(T_{avg} - 27) \tag{18}$$

$$k_a = 0.02624 + 0.0000758(T_{avg} - 27) \tag{19}$$

$$\mu_a = [1.983 + 0.00184(T_{avg} - 27)] \times 10^{-5} \tag{20}$$

The heat transfer from the glass cover to the ambient is caused by the wind flow in the atmosphere. The following correlation is used to predict the corresponding heat transfer coefficient

$$h_{wd} = 2.8 + 3.3V_{wd} \tag{21}$$

The following relation is used to calculate the radiation heat transfer coefficient between the glass cover and sky,

$$h_{rn,\,gl\,-\,sy} = \sigma\varepsilon_{gl}(T_{gl} + T_{sy})(T_{gl}^2 + T_{sy}^2) \tag{22}$$

$$T_{sy} = 0.0552T_{amb}^{1.5} \tag{23}$$

The heat transfer from the absorber plate to the glass cover caused by natural convection is estimated. The following correlation is used to predict the corresponding heat transfer coefficient

$$h_{nc} = \frac{k_a}{Z_3}Nu_{nc} \tag{24}$$

$$Nu_{nc} = 1 + 1.44\left[1 - \frac{1708(sin1.8\varphi)^{1.6}}{Ra\,\cos\varphi}\right]\left[1 - \frac{1708}{Ra\,\cos\varphi}\right]^{+} + \left[\left(\frac{Ra\,\cos\varphi}{5830}\right)^{1/3} - 1\right]^{+} \tag{25}$$

In the above equation, φ represents the air heater tilt angle and +sign in the super script indicates last parameter to be considered when the positive value arrives. The Ra represents the Rayleigh number and calculated by relation as shown in Eq. (26).

$$Ra = \frac{g\beta(T_{pl} - T_{gc})Z_3}{\alpha_a\nu_a} \tag{26}$$

To evaluate the radiation heat transfer coefficient between the absorber plate and glass cover, the following relation is used.

$$h_{rn,\,pl\,-\,gc} = \frac{\sigma(T_{pl}^2 + T_{gc}^2)(T_{pl} + T_{gc})}{\frac{1}{\varepsilon_{pl}} + \frac{1}{\varepsilon_{gc}} - 1} \tag{27}$$

The heat, transferred from the absorber plate to the flowing air in the duct, causes the convective heat transfer. The following correlation is used to predict the corresponding heat transfer coefficient

$$h_{cn,\,pl\,-\,f} = \frac{k_a}{D_h}Nu_{cn,pl\,-\,f} \tag{28}$$

In the above Eq. (28), the Nusselt number ($Nu_{c,pl\,-\,f}$)can be expressed as [10]

$$Nu_{cn,pl\,-\,f} = 0.001047\mathrm{Re}^{1.3186}\left(\frac{e}{D_h}\right)^{0.3772}\left(\frac{\alpha}{90}\right)^{-0.1198} \tag{29}$$

In the above equation, the hydraulic diameter of the SAH duct is calculated by using the relation as expressed in Eq. (30).

$$D_h = \frac{4(W_d Z_2 - N_o h_{fin} t_{fin})}{2(W_d + Z_2) + N_o(h_{fin} + t_{fin})} \tag{30}$$

To evaluate the radiation heat transfer coefficient between the absorber plate and back plate, the following relation can be used.

$$h_{rn,\,pl\,-\,be} = \frac{\sigma(T_{pl}^2 + T_{be}^2)(T_{pl} + T_{be})}{\frac{1}{\varepsilon_{pl}} + \frac{1}{\varepsilon_{be}} - 1} \tag{31}$$

The heat, transferred from the back plate to the flowing air in the duct, causes the convective heat transfer. The following correlation is used to predict the corresponding heat transfer coefficient [21]

$$h_{cn,\,be\,-\,f} = \frac{k_a}{D_h}Nu_{c,be\,-\,f} \tag{32}$$

$$Nu_{cn,be\,-\,f} = 0.116(\mathrm{Re}_a^{2/3} - 125)\mathrm{Pr}^{1/3} + \left[1 + \left[\frac{Dh}{L}\right]^{\frac{2}{3}}\right]\left[\frac{\mu_a}{\mu_w}\right]^{0.14} \quad (2300 < \mathrm{Re}_a < 6000) \tag{33}$$

$$Nu_{cn,be\,-\,f} = 0.018\mathrm{Re}_a^{0.8}\mathrm{Pr}^{0.4} \quad (\mathrm{Re}_a > 6000) \tag{34}$$

2.4. Pressure drop and pumping power requirement for SAH channel

The friction, occurred between the flowing air and SAH components, causes the pressure drop inside the duct. The following relations are used to evaluate the drop in pressure and pumping power requirement at various operating conditions.

$$P_{mech} = \frac{\dot{m}_a \times (\Delta P_a)}{\rho_a} \tag{35}$$

$$\Delta P_a = \frac{2f_r L_d V^2 \rho_a}{D_h} \tag{36}$$

In the above equation the friction factor is calculated by following relation [10].

$$f_r = 0.14408\mathrm{Re}_a^{-0.17103}\left(\frac{e}{D_h}\right)^{0.1765}\left(\frac{\alpha}{90}\right)^{0.1185} \tag{37}$$

The total pressure drop occurred inside the duct due to the combined effect of arc shaped roughness with fins and a baffle is evaluated by using the relation as follows [26].

$$\Delta P_a = (1.465 \times 10^{-5})\mathrm{Re}_a^{1.94}\left(\frac{W_B}{D_h}\right)^{2.6}\left(\frac{L_d}{L_B}\right)^{1.2} + \frac{2f_r L_d V^2 \rho_a}{D_h} \tag{38}$$

2.5. Thermal performance of SAH

2.5.1. First law efficiency

From the first law of thermodynamics, useful energy gain for the working fluid is calculated by the equation [31]

$$\eta_I = \frac{Q_u}{A_{pl} \times S} = \frac{\dot{m}_a C_{p_a}(T_{fo} - T_{fi})}{A_{pl} \times S} \tag{39}$$

2.5.2. Exergy efficiency

Exergy based analysis provides the maximum feasibility of energy conversion of thermal systems with respect to ambient conditions. In this work, loss-based exergy investigation is carried out to optimize the design and operating parameters. Fig. 2 shows the exergy balance for various components of the SAH and following expressions are used for

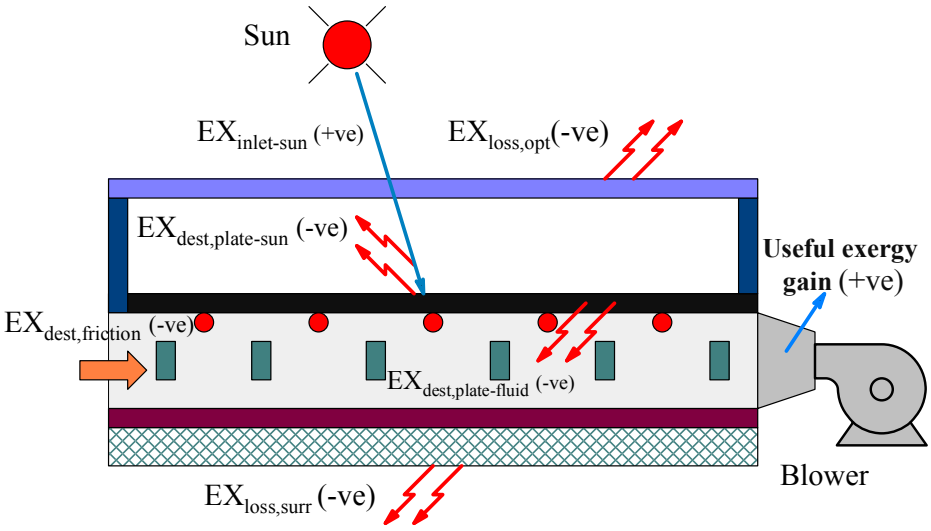

Fig. 2. Exergy destruction in each component of solar air heater.

estimating the exergy gain and destruction [32].

$$\Sigma \dot{E}x_{in} - \Sigma \dot{E}x_{out} = \Sigma \dot{E}x_{losses} \tag{40}$$

$$\eta_{II} = 1 - \frac{\Sigma \dot{E}_{loss}}{\Sigma \dot{E}_{in}} \tag{41}$$

$$\Sigma \dot{E}_{in} = IA\left[1 - \frac{4}{3}\left(\frac{T_{amb}}{T_{sun}}\right) + \frac{1}{3}\left(\frac{T_{amb}}{T_{sun}}\right)^4\right] \tag{42}$$

$$\Sigma \dot{E}_{loss} = (\dot{E}_{optl-loss}) + (\dot{E}_{Q-loss}) + (\dot{E}_{fr-loss}) + \left(\dot{E}_{T_{pl},T_{sun}-loss}\right) + \left(\dot{E}_{T_{pl},T_f-loss}\right) \tag{43}$$

$$\dot{E}_{optl-loss} = IA(1 - \alpha_{pl}\tau_{gl})\left[1 - \frac{4}{3}\left(\frac{T_{amb}}{T_{sun}}\right) + \frac{1}{3}\left(\frac{T_{amb}}{T_{sun}}\right)^4\right] \tag{44}$$

$$\dot{E}_{Q-loss} = U_L A(T_{pl} - T_{amb})\left[1 - \left(\frac{T_{amb}}{T_{pl}}\right)\right] \tag{45}$$

where

$$U_L = U_{top} + U_{be} \tag{46}$$

$$U_L = \left[\frac{1}{(h_{rn,pl-gl} + h_{nc})} + \frac{1}{(h_{rn,gl-sy} + h_{wd})}\right]^{-1} \tag{47}$$

$$\dot{E}_{T_{pl},T_{sun}-loss} = IA_{pl}\alpha_{pl}\tau_{gl}\left[1 - \frac{4}{3}\left(\frac{T_{amb}}{T_{sun}}\right) + \frac{1}{3}\left(\frac{T_{amb}}{T_{sun}}\right)^4 - \left(1 - \frac{T_{amb}}{T_{pl}}\right)\right] \tag{48}$$

$$\dot{E}_{T_{pl},T_{amb}-loss} = SA_{pl}\eta_{th}T_{amb}\left[\left(\frac{1}{T_f}\right) - \left(\frac{1}{T_{pl}}\right)\right] \tag{49}$$

$$(\dot{E}_{fr-loss}) = \frac{T_{amb}\dot{m}_a\Delta p_a}{\rho_f T_f} \tag{50}$$

Loss based exergy efficiency can be calculated by invoking values from Eqs. (42) to (50) in to Eq. (41).

2.6. Theoretical methodology

MATLAB code has been developed to solve energy balance Eqs. (13)–(16). Design and operating conditions are given as initial input for solving above equations. Heat transfer coefficient and thermo physical properties are calculated using the Eqs. (17)–(34). Using matrix inversion techniques, the average SAH components and air temperature are calculated [33]. Further, obtained values are compared with assumed values and updated if the deviation is greater than 0.01 °C. When the convergence is reached, temperature values are used to energy and exergy efficiency using the Eqs. (35)–(50).

3. Results and discussions

The loss based exergetic performance analysis is carried out for the proposed SAH with desired range of design parameters and operating conditions as shown in Table.1.The variations of mass flow rate, length, width of baffles and number of fins are optimized based on Genetic algorithm [27]. It invokes the concept of evolutionary nature for performing the probability of global search For optimizing the design parameters of SAH, the objective function with its constraints is developed and fed to the MATLAB GA tool box.

$$\text{Maximize } \eta_{ex} = Equation\,(87)$$

$$\text{conditions to}$$

$$\begin{cases} 0.01 \leqslant \dot{m} \leqslant 0.08 \\ 0.005 \leqslant W_B \leqslant 0.015 \\ 0.2 \leqslant L_B \leqslant 0.4 \\ 2 \leqslant N_O \leqslant 8 \end{cases}$$

From the analysis, the optimized design parameters are identified and their influences on exergetic performance of SAH are discussed in the following sections.

Optimum values are

$$\begin{cases} \eta_{ex} = 5.22\% \\ \dot{m} = 0.012\ kg/s \\ W_B = 0.015\ m \\ L_B = 0.2\ m \\ N_o = 8 \end{cases}$$

3.1. Validation of present theoretical model

To validate the theoretical model, developed based on the energy

Table 1
Design and operating conditions used for exergy analysis.

Parameters	Base Values
Fixed Design and operating conditions of SAH	
Length of the air flow path, L_d	1.5 m
Width of the air flow path, Wd	1 m
Height of air heater channel, Z_2	0.03 m
Space between absorber plate and glass cover (d),	0.05 m
Insulation thickness of, δ_{in}	0 0.05 m
Thermal conductivity of insulation k_i	0.037 W/m K
Atmospheric temperature, T_{amp}	300 K
Wind velocity, V_{wd}	1.5 m/s
Rib height-to-duct hydraulic diameter ratio, (e/D_h)	0.0422
Flow-attack-angle, $(\alpha/90)$	0.333
Relative roughness pitch (P/e)	10
Height of the extended surface	0.03 m
Thickness of the extended surface	0.001 m
Thermal conductivity of the extended surface (k_{fin})	14.9 W/mK
Intensity of solar heat flux, (S)	800 W/m^2
Absorber plate - emissivity ε_p	0.9
Bottom plate- emissivity, ε_b	0.9
Glass cover -emissivity, ε_g	0.88
Effective transmittance absorptance product, $\tau\alpha_p$	0.8
Range of Design and operating parameters	
Reynolds Number (Re)	2900–17,000
Width of the Baffle (W_B)	0.005–0.015 m
Length of the Baffle (L_B)	0.2–0.4 m
Number of fins (N_O)	2–10

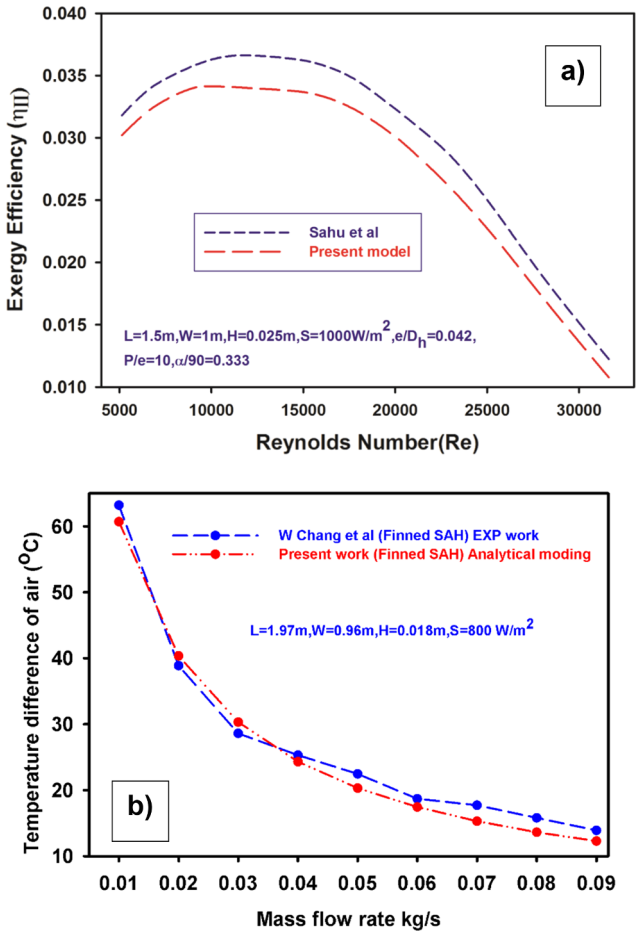

Fig. 3. Validation of mathematical model (a) based on Exergy efficiency (b) Based on outlet temperature.

balance equations of each component of the SAH and code developed in the MATLAB, present simulation results are compared with the results of Sahu et al. [10] at identical collector design and operating conditions. The comparison results as shown in Fig. 3a ensures the reliability of the present model with the average absolute deviation of 7.56%. This variation is due to fact that the energy inflow from sun to absorber plate is calculated by considering Petla's relations in this theoretical model.

Further, validity of mathematical model results has been compared with experimental results as shown in Fig. 3b [34] .This figure shows the outlet temperature of the finned SAH and ensures that the model has good agreement with previous results. It can also be used to evaluate the performance of arc shaped roughened SAH integrated with fins and baffles.

3.2. Effect of mass flow rate on exergy destruction and losses

Fig. 4(a) – (f) illustrate the relationship between the mass flow rate and exergy efficiency with exergy destruction and losses for optimized design conditions. In Fig. 4(a), the exergy efficiency increases with increasing mass flow rate steeply and attains the maximum value of 5.22% at mass flow rate of 0.012 kg/s and then further it decreases linearly. It is also observed that the exergy losses to the surrounding decreases steeply when mass flow rate ascends but it has no effect on the optical exergy loss as it depends on material properties of the glass as shown in Fig. 4(b) and (c).

As seen from the Fig. 4(d) and (f), the exergy destruction between plate and Sun and due to friction, increase with ascending trend of mass flow rate. It is due to the fact that at higher mass flow rate, the temperature of the absorber plate declines due to more heat transfer to the fluid. It is evidenced, from Eq. (7) that the decreasing the absorber temperature enhances the exergy destruction between plate and Sun. It is also known that when mass flow rate increases, the pressure drop across the duct also increases thereby resulting in increase in exergy destruction due to friction.

As the mass flow rate ascends, the exergy destruction between the plate and fluid increases steeply and reaches the maximum value as shown in Fig. 4(e). Further increase in mass flow rate descends the destruction steadily. The optimum mass flow rate is found to be 0.012 kg/s for attaining the maximum exergy efficiency. This is due to the fact that the exergy destruction due to heat loss to ambient enormously descends as of decrease in temperature of solar air heater components. During that time, magnitude of all other exergy destruction and losses, following ascending trend, are lower than that of exergy destruction losses to the surrounding.

3.3. Effect of baffle width on exergy destruction and losses

Fig. 5(a)–(f) show the influence of width of baffles on the exergy efficiency and other exergy destruction and losses. At optimized conditions, the exergy efficiency linearly increases with the width of baffles as shown in Fig. 5(a). Maximum exergy efficiency is observed at the baffle width of 0.015 m. It is evident from Eq. (10) that the increase in the width results in better baffle efficiency. This increase in baffle efficiency enhances the convective heat transfer coefficient between air and absorber plate.

From the Fig. 5(b), it is also seen that the increase in baffle width reduces exergy losses to surrounding. Higher baffle width leads to more turbulence resulting in high flow separation and reattachment. As results, convective heat transfer is increased further. Further it reduces temperature of the air heater components where by reducing the exergy losses to surrounding. The effect of width of baffle on optical loss

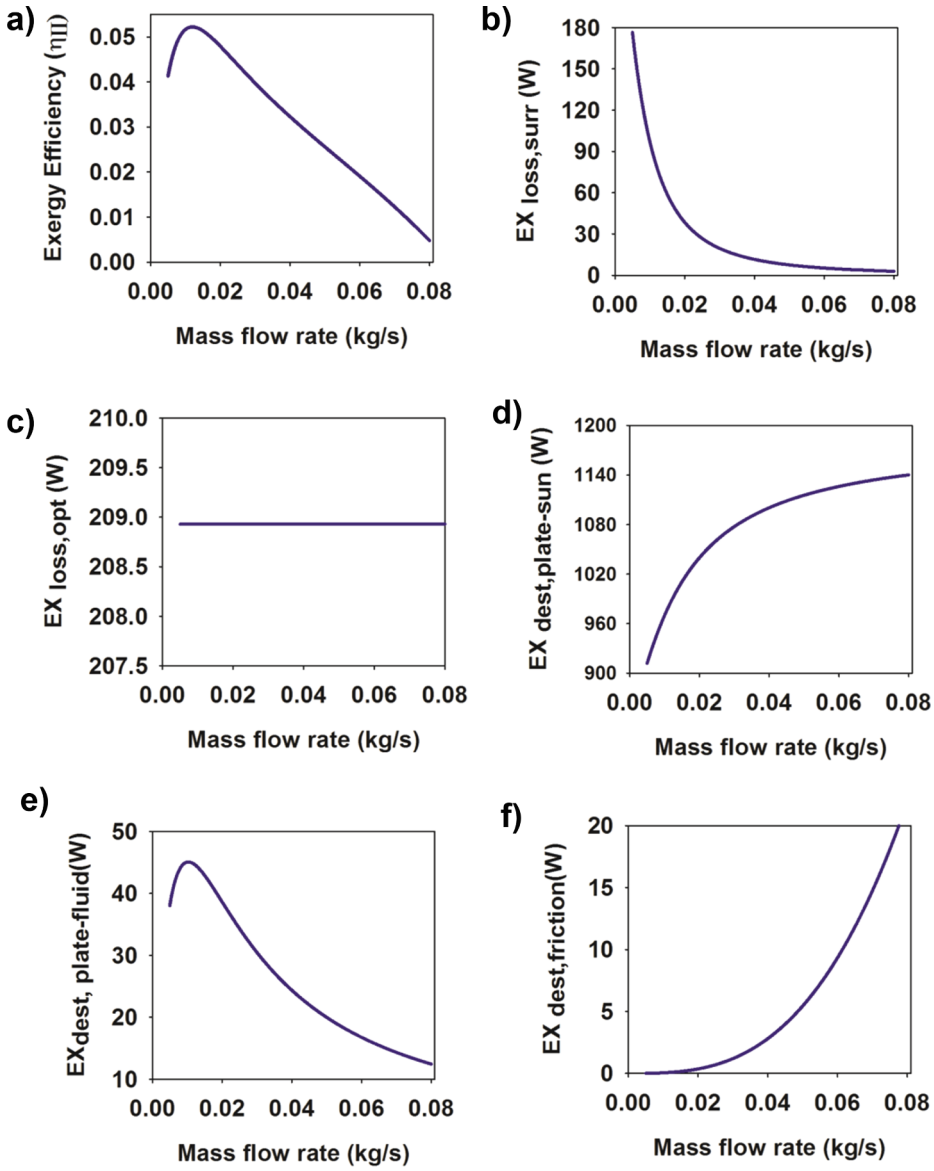

Fig. 4. Effect of mass flow rate on various Exergy destructions and losses.

remains constant as shown in Fig. 5(c). Fig. 5(d) emphasize the effect of baffle width on exergy destruction between plate and sun. When width of baffle increases, the destruction loss also increases. From the Eq. (10), it is evident that the plate temperature is higher at lower baffle width resulting in low exergy destruction and vice versa.

As shown in Fig. 5(e) and (f), when the baffle width increases, the exergy destruction between plates and fluid decreases sharply as the fluid temperature rises while absorber temperature decreases rapidly. Exergy destruction due to fluid friction increases when the baffle width increases. Because of more resistance to fluid flow offered by baffle, the pressure drop increases inside the duct.

3.4. *Effect of baffle length on exergy destruction and losses*

Fig. 6(a)–(f) point up the relationship between the length of the baffle and exergy efficiency with exergy destruction and losses for optimized design conditions. Fig. 6(a) shows the liner relationship between the length of the baffle and exergy efficiency. At lower baffle length of 0.2 m, the maximum exergy is observed. Further increase in baffle length decreases the exergy efficiency.

The subsequent Fig. 6(b)–(f) represent the relationship between the exergy destruction and losses as function of length of the baffle. Exergy losses to the surrounding and exergy destruction between plate and fluid increase when the length of baffle increases. When the length of baffle increases, number of baffle along the flow path decreases. As a result, less turbulence effect induces poor mixing leading to higher exergy destruction. Except exergy optical loss, other destructions decrease smoothly when length increases. Consequently, plate temperature increases and flow friction decrease resulting in decrease in exergy destruction.

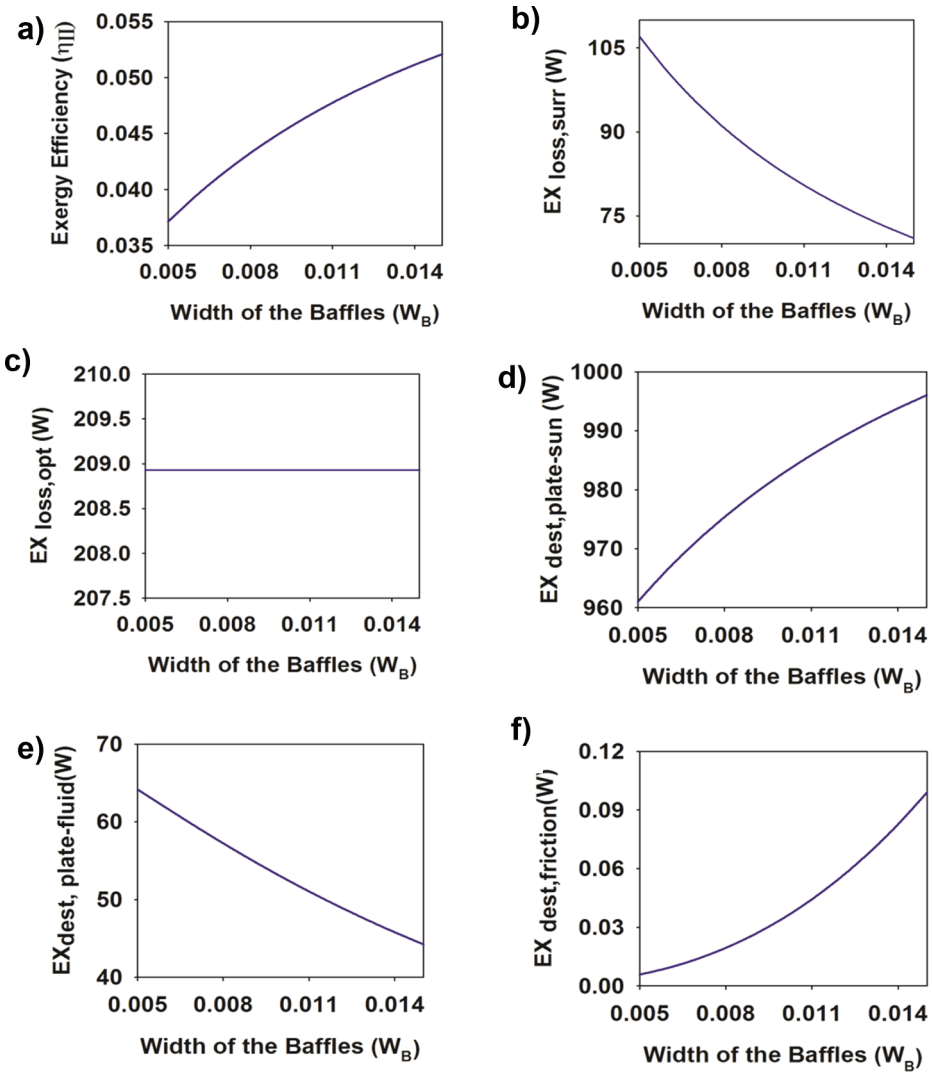

Fig. 5. Effect of Baffle width on various Exergy destructions and losses.

3.5. Effect of number of fins on exergy destruction and losses

Fig. 7(a)–(f) show the relationship between the number of fins and exergy efficiency with exergy destruction and losses for optimized design parameters. When the number of fins increases, the exergy efficiency also increases. The maximum exergy efficiency is observed as 5.22% when the number of fins is 8 as shown in Fig. 7(a). The subsequent Fig. 7(b)–(f) represent the relationship between the exergy destruction and losses as function of number of fins. Exergy losses to the surrounding and exergy destruction between plate and fluid decreases when the number of fins increases. When the number of fins increases, the surface area for heat transfer increases. As a result, more heat transfer to the flowing air. Further, attached baffle with fins induces more turbulence leading to more swirl. Except exergy optical loss, other destructions increases linearly when number of fins increases. Consequently, the plate temperature decreases and flow friction increases resulting in more exergy destruction.

3.6. Effect of operational and geometrical parameter on exergy efficiency

Fig. 8 shows the significant effect of mass flow rate and width of the baffle on exergy efficiency. It confirms the optimized flow rate for various baffle width. From the figure, it is observed that the maximum exergy efficiency of 3.5%, 4.1%, 4.5%, 4.9% and 5.2% are obtained for the width of 0.005 m, 0.007 m, 0.01 m, 0.012 m, 0.015 m respectively, when the mass flow rate ranges from 0.0272 kg/s to 0.013 kg/s. From these vales, it is inferred that the maximum exergy is obtained at higher baffle width for the corresponding range of mass flow rate.

Fig. 9 illustrates the considerable effect of mass flow rate and length of the baffle on exergy efficiency. It shows the optimized flow rate for various baffle length. From the figure, it is noted that the maximum exergy efficiency of 3.66%, 4.2%, and 5.2% are obtained for the length of 0.4 m, 0.3 m, and 0.2 m respectively, when the mass flow rate ranges from 0.0197 kg/s to 0.0126 kg/s. From these vales, it is conclude d that the maximum exergy is obtained at lower baffle length for the corresponding range of mass flow rate.

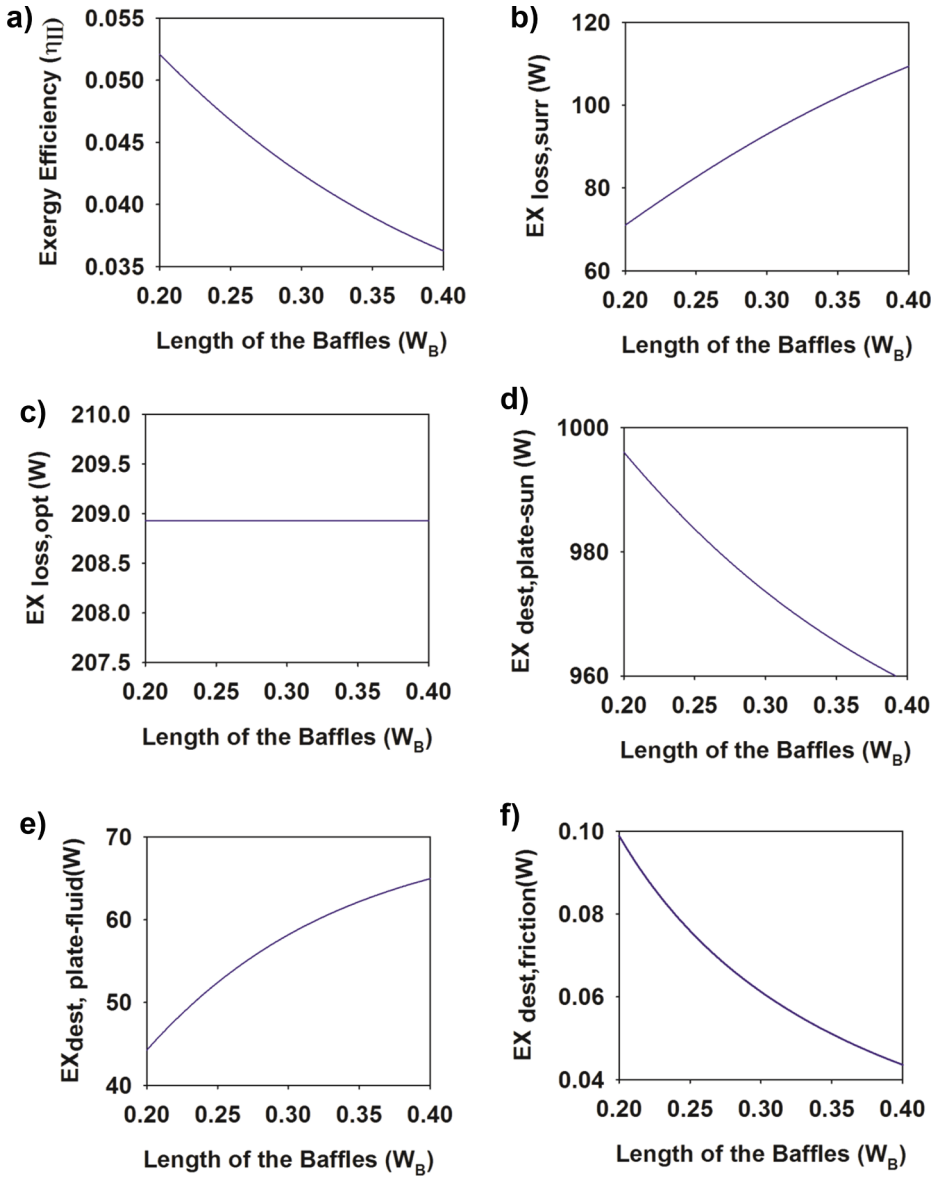

Fig. 6. Effect of Baffle Length on various Exergy destructions and losses.

Fig. 10 point up the significant effect of mass flow rate and the number of fins on exergy efficiency. It illustrates the optimized flow rate for number of fins. From the figure, it is prominent that the maximum exergy efficiency of 5.2%, 4.8%, 4.2% and 3.4% are obtained for the number of fins of 8, 6, 4, 2 respectively, when the mass flow rate ranges from 0.013 kg/s to 0.019 kg/s. From these values, it is inferred that the maximum exergy is obtained at more number of fins for the corresponding range of mass flow rate.

Fig. 11 highlights the significant effect of width of the baffle and length of the baffle on exergy efficiency at optimized mass flow rate. From the figure, it is evident that the maximum exergy efficiency of 5.2% is obtained for the baffle length and width of 0.2 m, 0.15 m respectably. It is also observed that the higher width and lower length values provide the maximum exergy efficiency at optimized flow rate. Fig. 12 point up the influence of number of fins and width of baffle on exergy efficiency. It is clear that the more number of fins with larger baffle width provides the maximum exergy efficiency due to more heat transfer area and flow vortices.

Fig. 13 compares the present results with results available in the literature at identical operating conditions. From this Fig. 13, it is concluded that the arc shaped rib roughened solar air heater integrated with fins and baffles enhanced the exergy efficiency by 2.8 times as compared with arc shaped rib roughened SAH analysed by Sahu et al. [10] and by 1.25 times when compared with fins and baffled SAH

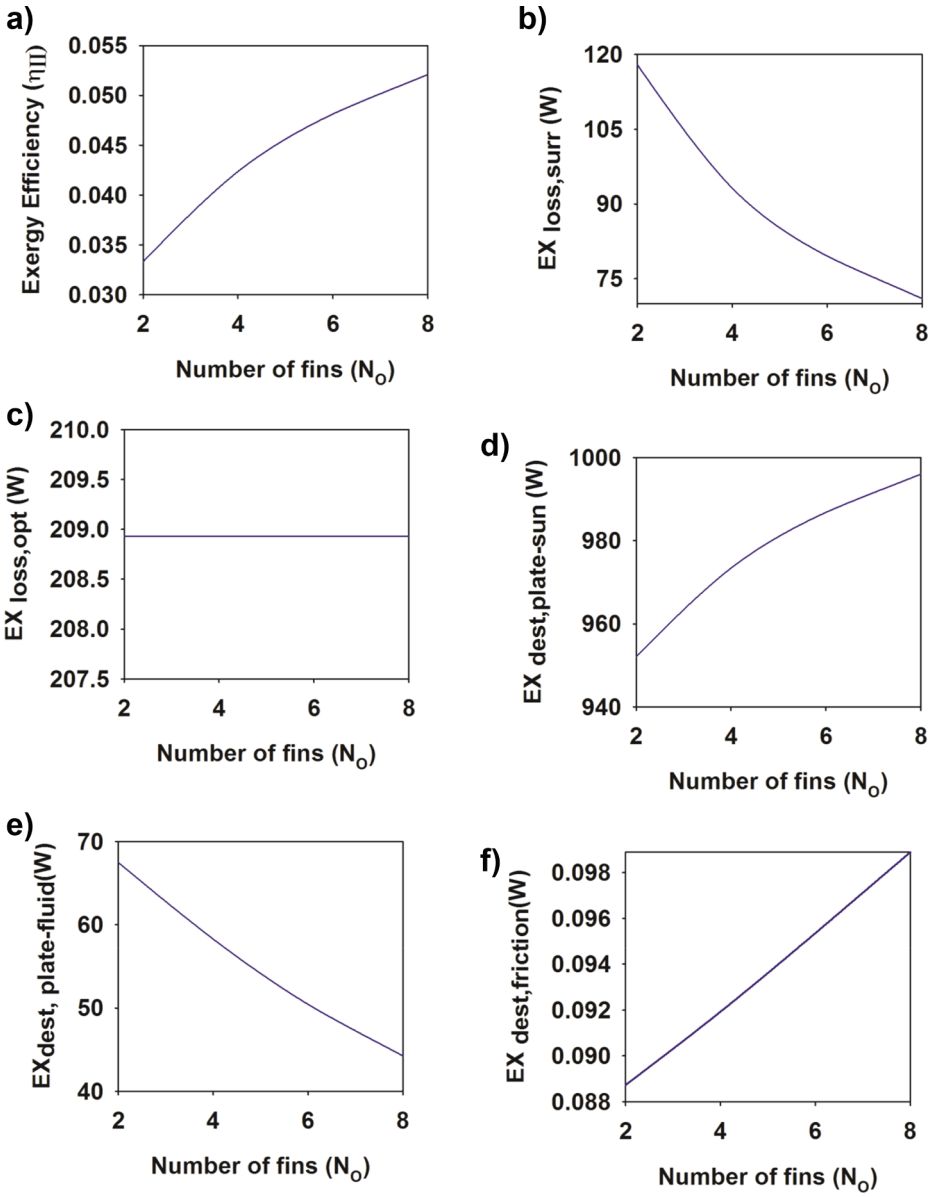

Fig. 7. Effect of Number of fins on various Exergy destructions and losses.

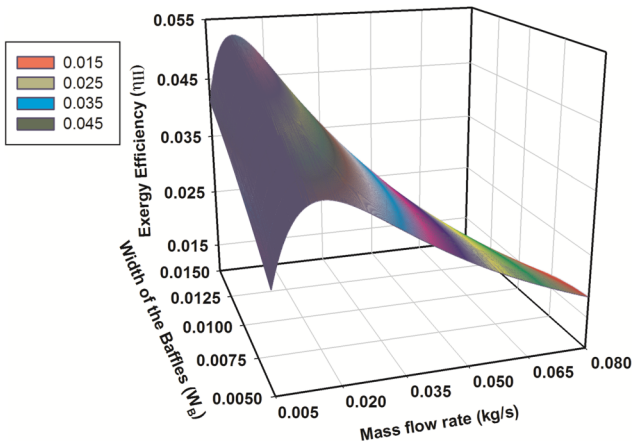

Fig. 8. Exergy efficiency as a function of mass flow rate and Width of the Baffle.

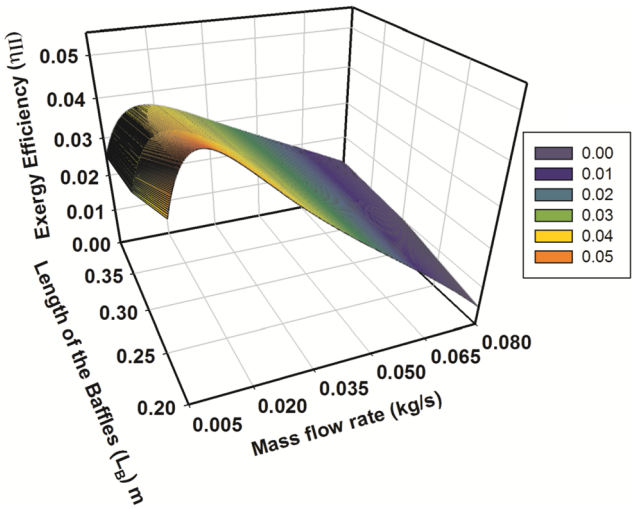

Fig. 9. Exergy efficiency as a function of mass flow rate and Length of the Baffle.

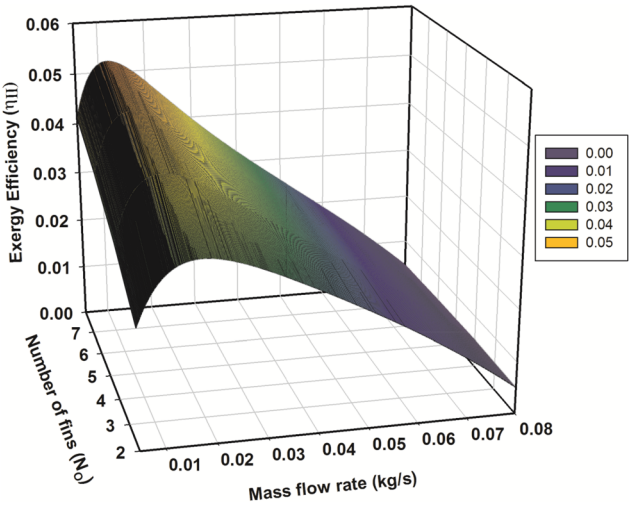

Fig. 10. Exergy efficiency as a function of mass flow rate and Number of fins.

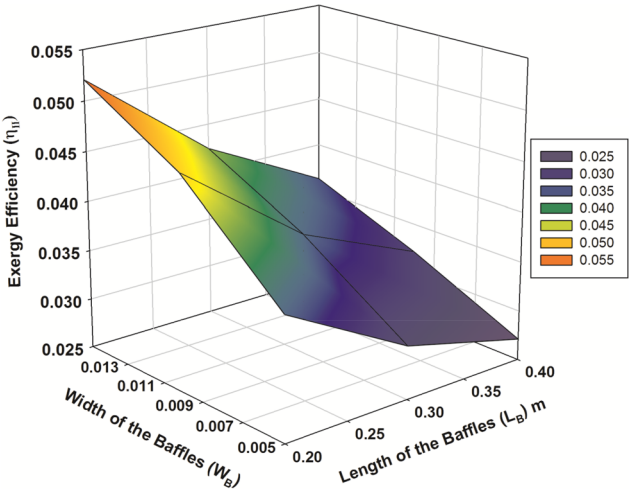

Fig. 11. Exergy efficiency as a function of Width and Length of the Baffles.

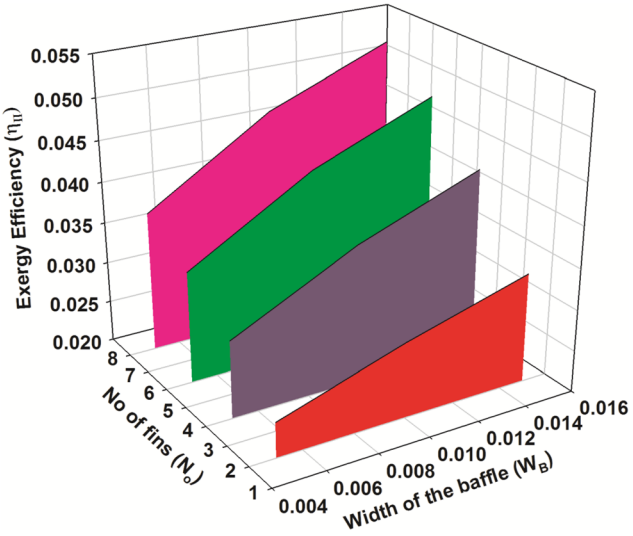

Fig. 12. Exergy efficiency as a function of Number of fins and Width of the Baffle.

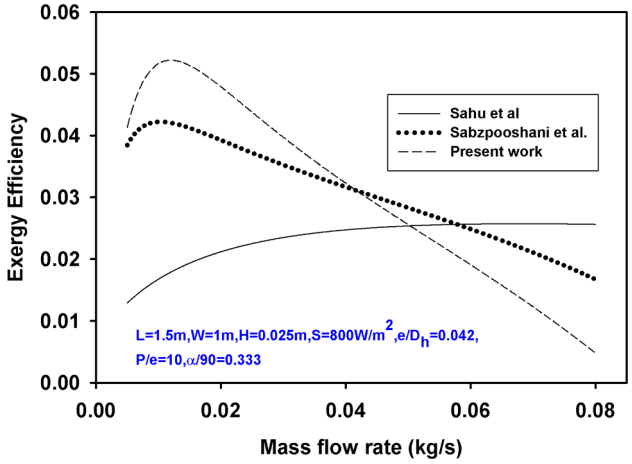

Fig. 13. Exergy based performance comparison between SAHs.

investigated by Sabzpooshani et al. [26] at the optimum mass flow rate of 0.012 kg/s. It is also observed that exergy efficiency of the proposed SAH performs better up to the mass flow rate of 0.042 kg/s.

4. Conclusions

This work focused on the optimizing the design and operating parameters of SAH based on exergy efficiency using Genetic algorithm. The numerical simulation code has been compared with theoretical results available in the literature. From the present results, the following conclusions are obtained

- For design and operating parameters, the optimum values obtained for baffle width, baffle length, numbers of fins and mass flow rate are 0.015 m, 0.2 m, 8 and 0.012 kg/s respectively. Above optimized conditions, the exergy efficiency of SAH is 5.2%.
- When mass flow rate is exceeded the optimum value, more exergy destruction between the plate and Sun is observed.
- When the baffle width is increased, less exergy destruction from plate to fluid and less destruction due to ambient heat loss are noted even though significant rise in exergy destruction between plate and sun is observed.
- If the length of the baffle is increased, the destruction between plate and fluid and destruction due to heat loss to surrounding are increased
- When the numbers of fins are increased, destruction due to heat loss to the surroundings and destruction between plate and fluid are significantly decreased even though there is rise in other two destruction losses.

Declaration of Competing Interest

The authors declare that they have no known competing financial interests or personal relationships that could have appeared to influence the work reported in this paper.

Appendix A. Supplementary material

Supplementary data to this article can be found online at https://doi.org/10.1016/j.applthermaleng.2020.115316.

References

[1] G.D. Towards, Ren 21 – Renewable Global Futures Report, 2017. https://doi.org/10.1109/JRPROC.1918.217382.

[2] A. Kumar, R.P. Saini, J.S. Saini, Effect of roughness width ratio in discrete Multi v-shaped rib roughness on thermo-hydraulic performance of solar air heater, Heat Mass Transf. Und Stoffuebertragung. 51 (2014) 209–220, https://doi.org/10.1007/s00231-014-1407-0.

[3] K.R. Aharwal, C.B. Pawar, A. Chaube, Heat transfer and fluid flow analysis of artificially roughened ducts having rib and groove roughness, Heat Mass Transf. Und Stoffuebertragung. 50 (2014) 835–847, https://doi.org/10.1007/s00231-014-1292-6.

[4] S. Skullong, C. Thianpong, P. Promvonge, Effects of rib size and arrangement on forced convective heat transfer in a solar air heater channel, Heat Mass Transf. Und Stoffuebertragung. 51 (2015) 1475–1485, https://doi.org/10.1007/s00231-015-1515-5.

[5] S. Skullong, P. Promvonge, C. Thianpong, M. Pimsarn, Thermal performance in solar air heater channel with combined wavy-groove and perforated-delta wing vortex generators, Appl. Therm. Eng. 100 (2016) 611–620, https://doi.org/10.1016/j.applthermaleng.2016.01.107.

[6] S. Skullong, P. Promvonge, C. Thianpong, N. Jayranaiwachira, M. Pimsarn, Heat transfer augmentation in a solar air heater channel with combined winglets and wavy grooves on absorber plate, Appl. Therm. Eng. 122 (2017) 268–284, https://doi.org/10.1016/j.applthermaleng.2017.04.158.

[7] T. Salameh, A.H. Alami, B. Sunden, Experimental investigation of the effect of variously-shaped ribs on local heat transfer on the outer wall of the turning portion of a U-channel inside solar air heater, Heat Mass Transf. Und Stoffuebertragung. 52 (2016) 539–546, https://doi.org/10.1007/s00231-015-1541-3.

[8] R. Kumar, A. Kumar, A. Sharma, R. Chauhan, M. Sethi, Experimental study of heat transfer enhancement in a rectangular duct distributed by multi V-perforated baffle of different relative baffle width, Heat Mass Transf. Und Stoffuebertragung. 53 (2017) 1289–1304, https://doi.org/10.1007/s00231-016-1901-7.

[9] R.K. Ravi, R.P. Saini, Nusselt number and friction factor correlations for forced convective type counter flow solar air heater having discrete multi V shaped and staggered rib roughness on both sides of the absorber plate, Appl. Therm. Eng. 129 (2018) 735–746, https://doi.org/10.1016/j.applthermaleng.2017.10.080.

[10] M.K. Sahu, R.K. Prasad, Exergy based performance evaluation of solar air heater with arc-shaped wire roughened absorber plate, Renew. Energy. 96 (2016) 233–243, https://doi.org/10.1016/j.renene.2016.04.083.

[11] A. Kumar, A. Layek, Energetic and exergetic performance evaluation of solar air heater with twisted rib roughness on absorber plate, J. Clean. Prod. 232 (2019) 617–628, https://doi.org/10.1016/j.jclepro.2019.05.363.

[12] M. Abuşka, S. Şevik, Energy, exergy, economic and environmental (4E) analyses of flat-plate and V-groove solar air collectors based on aluminium and copper, Sol. Energy 158 (2017) 259–277, https://doi.org/10.1016/j.solener.2017.09.045.

[13] M. Abuşka, Energy and exergy analysis of solar air heater having new design absorber plate with conical surface, Appl. Therm. Eng. 131 (2018) 115–124, https://doi.org/10.1016/j.applthermaleng.2017.11.129.

[14] M.M. Matheswaran, T.V. Arjunan, D. Somasundaram, Energetic, exergetic and enviro-economic analysis of parallel pass jet plate solar air heater with artificial roughness, J. Therm. Anal. Calorim. (2018), https://doi.org/10.1007/s10973-018-7727-4.

[15] M.M. Matheswaran, T.V. Arjunan, D. Somasundaram, Analytical investigation of exergetic performance on jet impingement solar air heater with multiple arc protrusion obstacles, J. Therm. Anal. Calorim. 137 (1) (2019) 253–266.

[16] A.P. Omojaro, L.B.Y. Aldabbagh, Experimental performance of single and double pass solar air heater with fins and steel wire mesh as absorber, Appl. Energy 87 (2010) 3759–3765, https://doi.org/10.1016/j.apenergy.2010.06.020.

[17] K. Kulkarni, K.Y. Kim, Comparative study of solar air heater performance with various shapes and configurations of obstacles, Heat Mass Transf. Und Stoffuebertragung. 52 (2016) 2795–2811, https://doi.org/10.1007/s00231-016-1788-3.

[18] E.K. Akpinar, F. Koçyiğit, Energy and exergy analysis of a new flat-plate solar air heater having different obstacles on absorber plates, Appl. Energy 87 (2010) 3438–3450, https://doi.org/10.1016/j.apenergy.2010.05.017.

[19] A. Kumar, R. Kumar, R. Maithani, R. Chauhan, S. Kumar, R. Nadda, An experimental study of heat transfer enhancement in an air channel with broken multi type V-baffles, Heat Mass Transf. Und Stoffuebertragung. 53 (2017) 3593–3612, https://doi.org/10.1007/s00231-017-2089-1.

[20] K. Mohammadi, M. Sabzpooshani, Comprehensive performance evaluation and parametric studies of single pass solar air heater with fins and baffles attached over the absorber plate, Energy 57 (2013) 741–750, https://doi.org/10.1016/j.energy.2013.05.016.

[21] K. Mohammadi, M. Sabzpooshani, Appraising the performance of a baffled solar air heater with external recycle, Energy Convers. Manag. 88 (2014) 239–250, https://doi.org/10.1016/j.enconman.2014.08.009.

[22] P.T. Saravanakumar, D. Somasundaram, M.M. Matheswaran, Thermal and thermo-hydraulic analysis of arc shaped rib roughened solar air heater integrated with fins and baffles, Sol. Energy 180 (2019) 360–371, https://doi.org/10.1016/j.solener.2019.01.036.

[23] D. Alta, E. Bilgili, C. Ertekin, O. Yaldiz, Experimental investigation of three different solar air heaters: energy and exergy analyses, Appl. Energy 87 (2010) 2953–2973, https://doi.org/10.1016/j.apenergy.2010.04.016.

[24] D. Somasundaram, A. Mani, M. Kamaraj, Experimental investigation of thermal performance of metal foam wicked flat heat pipe, Exp. Therm. Fluid Sci. 82 (2017) 482–492, https://doi.org/10.1016/j.expthermflusci.2016.12.006.

[25] F. Bayrak, H.F. Oztop, A. Hepbasli, Energy and exergy analyses of porous baffles inserted solar air heaters for building applications, Energy Build. 57 (2013) 338–345, https://doi.org/10.1016/j.enbuild.2012.10.055.

[26] M. Sabzpooshani, K. Mohammadi, H. Khorasanizadeh, Exergetic performance evaluation of a single pass baffled solar air heater, Energy 64 (2014) 697–706, https://doi.org/10.1016/j.energy.2013.11.046.

[27] M. Ansari, M. Bazargan, Optimization of flat plate solar air heaters with ribbed surfaces, Appl. Therm. Eng. 136 (2018) 356–363, https://doi.org/10.1016/j.applthermaleng.2018.02.099.

[28] A.Ş. Şahin, Optimization of solar air collector using genetic algorithm and artificial bee colony algorithm, Heat Mass Transf. Und Stoffuebertragung. 48 (2012) 1921–1928, https://doi.org/10.1007/s00231-012-1038-2.

[29] S. Chamoli, ANN and RSM approach for modeling and optimization of designing parameters for a v down perforated baffle roughened rectangular channel, Alexandria Eng. J. 54 (2015) 429–446, https://doi.org/10.1016/j.aej.2015.03.018.

[30] H.K. Ghritlahre, R.K. Prasad, Exergetic performance prediction of solar air heater using MLP, GRNN and RBF models of artificial neural network technique, J. Environ. Manage. 223 (2018) 566–575, https://doi.org/10.1016/j.jenvman.2018.06.033.

[31] J.A. Duffie, W.A. Beckman, Solar Engineering of Thermal Processes, fourth ed., 2013. https://doi.org/10.1002/9781118671603.

[32] M.M. Matheswaran, T.V. Arjunan, D. Somasundaram, Analytical investigation of solar air heater with jet impingement using energy and exergy analysis, Sol. Energy 161 (2018) 25–37, https://doi.org/10.1016/j.solener.2017.12.036.

[33] C. Sivakandhan, T.V. Arjunan, M.M. Matheswaran, Thermohydraulic performance enhancement of a new hybrid duct solar air heater with inclined rib roughness, Renew. Energy 147 (2020) 2345–2357.

[34] W. Chang, Y. Wang, M. Li, X. Luo, Y. Ruan, Y. Hong, S. Zhang, The theoretical and experimental research on thermal performance of solar air collector with finned absorber, Energy Procedia 70 (2015) 13–22.